

Motion Error Compensation for Quad-rotor Miniature Unmanned Aerial Vehicle SAR Imaging

Song Zhou, Lei Yang, Gang Xu and Guoan Bi

School of Electrical and Electronic Engineering (EEE), Nanyang Technological University, Singapore, 639798, Singapore

Keywords: Quad-rotor Miniature Unmanned Aerial Vehicle (QMUAV), Synthetic Aperture Radar (SAR), Motion Error Compensation.

Abstract: Quad-rotor miniature unmanned aerial vehicle (QMUAV) synthetic aperture radar (SAR) is an ultra-small airborne SAR system. Because of lowing flying altitude and small size constraints, the motion errors of QMUAV-SAR are very complicated which introduces difficulty to the QMUAV-SAR imaging processing. To deal with this problem, an effective motion compensation approach for QMUAV-SAR is proposed. By establishing the relationship between the motion errors and the Doppler parameters of SAR echoes, the motion errors of QMUAV platform are extracted from the estimated Doppler rates. After the majority of the motion error being properly compensated, phase gradient autofocus (PGA) is employed to estimate and compensate the residual phase errors to further improve the focusing quality of the SAR image. Experimental results are provided and the image quality is evaluated to demonstrate the ability of achieving well focused image and high spacial resolutions of the proposed method.

1 INTRODUCTION

Quad-rotor miniature unmanned aerial vehicle (QMUAV) is a special kind of ultra-small unmanned aerial vehicle (UAV) that can be easily launched and landed in a space-constrained environment. Therefore, QMUAV has significant potentials in many practical applications, such as battlefield awareness, disaster monitoring and traffic control (Dydek et al., 2013; Lara et al., 2010; Zhao et al., 2015). Because synthetic aperture radar (SAR) is a microwave remote sensing technology with the capability of working all day and all weather, it has attracted growing interests in recent years. With current hardware technology, the antenna and the digital processor can be compacted into a very small and cheap flying platform for QMUAV SAR imaging. Being equipped with a SAR sensor on the UAV, high-resolution microwave images of the observed scene can be obtained to enhance its sensing capability under various environmental conditions (Coker and Tewfik, 2011; Zeng et al., 2015; Yang et al., 2015; Sun et al., 2013; Zhou et al., 2011).

For QMUAV SAR imaging, it is common that the flying path is easily and frequently disturbed by the atmospheric turbulence because of low flying altitude and small size constraints. The unknown motion er-

ror or the flying path deviation is usually significant enough to result in both serious defocusing and geometric distortion in the SAR image (Moreira, 1990). It is necessary to properly deal with the motion error problem to obtain a well focused image (Wahl et al., 1994; Xu et al., 2013; Zhang et al., 2012).

The motion errors can be measured and compensated by using on-board measurement equipment, such as the global positioning system (GPS) and the inertial navigation system (INS). With accurate flying path information, the impact of the motion error can be effectively reduced for obtaining desirable focusing quality of SAR image. Unfortunately, it is not possible to make use of accurate and expensive GPS and INS on board of the QMUAVs due to its constrains on size, weight and costs of the device. The motion error problem has appeared to be a difficult problem in the QMUAV SAR signal processing. In this paper, autofocus techniques are used to extract the motion error information from the SAR echoes. With the estimated motion error information, the motion compensation is accordingly carried out to improve the focusing quality of the final SAR image (Yang et al., 2013; Zhao et al., 2014; Zhou et al., 2013).

In this paper, experiment results of Ku-band QMUAV SAR are presented and the focusing quality

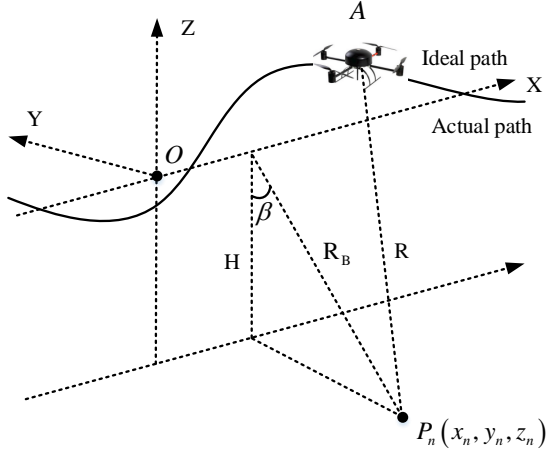


Figure 1: QMUAV SAR geometry.

of the QMUAV SAR image is evaluated. The paper is organized as follows. The QMUAV geometry and signal model are briefly introduced in section 2. The motion error of QMUAV and the impact are analysed in section 3. Then, the processing diagram integrated with autofocusing techniques is briefly described in section 4. In section 5, the QMUAV SAR system used in our experiment is briefly introduced and the experimental results are analyzed to demonstrate the validity of our motion error compensation algorithm. Finally, conclusion is provided in section 6.

2 SIGNAL MODEL

The geometry of the QMUAV SAR system is shown in Fig. 1. The radar is mounted on a QMUAV platform and is operated in strip-map mode. In ideal case, the antenna phase centre (APC) is supposed to move along a straight line (X axis) with a constant velocity, as indicated by the dashed line. The SAR echo signal can be expressed as the spectral form (Munson et al., 1983):

$$S(k, t) = \sum_{i \in S_C} A_i \exp[-jkR_i(t)] \quad (1)$$

where A_i is the backscattering coefficient, t is the azimuth time, and k is the wavenumber variable. The spectrum is the summation of echos from all scatterers (S_C) within the SAR antenna beam. $R_i(t)$ denotes i -th scatterer's range history during the QMUAV SAR flying along the expected path. When the QMUAV flies along the designated path, the SAR image can be obtained by using the back projection as (Desai and Jenkins, 1992)

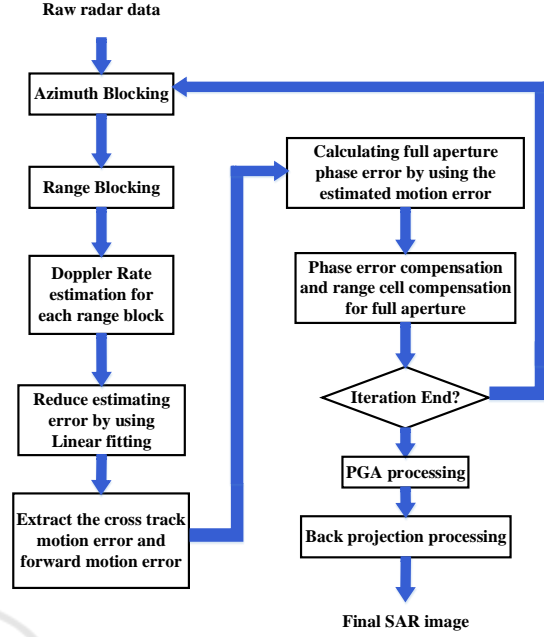


Figure 2: Main processing steps of the QMUAV SAR system.

$$I(x, y) = \int_{t_{\min}}^{t_{\max}} \int_{k_{\min}}^{k_{\max}} S(k, t) dk dt. \quad (2)$$

Because of the atmospheric turbulence in practice, the trajectory of the QMUAV platform seriously deviates from the designated path, as indicated by the solid curve. In this case, the range history $R_i(t)$ becomes $R_i(t) + \Delta R_i(t)$, and an additional phase modulation will be in $S(k, t)$. The error $\Delta R_i(t)$ will cause the SAR image degradation, such as smearing and deformation (Huang et al., 2011; Bao et al., 2012; Liao et al., 2013).

3 MOTION ERROR ANALYSIS

In the SAR processing, the range error and the motion error are closely related to the Doppler parameters of the SAR echoes. Because the quadratic coefficient of phase error is closely related to the motion error of the QMUAV, we first consider the Doppler rate parameter of the SAR echoes and establish the relation between motion error and the Doppler rate. Let β be the looking angle, as shown in Fig. 1. The ideal and the actual APC positions at t are $(v_0 t, 0, 0)$ and $(x(t), y(t), z(t))$, respectively, where v_0 is the ideal velocity. Then, the motion error can be denoted as $(x(t) - v_0 t, y(t), z(t))$, with $x(t) - v_0 t$ being the along-track motion error. $y(t)$ and $z(t)$ are the motion

errors along Y axis and Z axis. For an arbitrary scattering point $P_n(x_n, y_n, z_n)$, the range history $R(t)$ from the actual APC position to P_n is given by

$$R(t) = \sqrt{(x(t) - x_n)^2 + (y(t) - y_n)^2 + (z(t) - z_n)^2}. \quad (3)$$

The main problem in the analysis is that the along-track and cross-track motion errors are coupled together in (3). To facilitate the following discussion and derivation, the range history $R(t)$ is expanded into Taylor series with high order terms being ignored as follows (Xing et al., 2009)

$$R(t) \approx R_n + \frac{1}{2R_n}(x(t) - x_n)^2 + R_r(t) \quad (4)$$

where $R_n = \sqrt{y_n^2 + z_n^2}$ is the closest range of P_n with respect to the ideal trajectory. $R_r(t) = y(t) \sin \beta + z(t) \cos \beta$ is the cross-track motion error. In a SAR system, the phase modulation of the echoed signal arises from the range variation between radar and illuminated target and the corresponding phase history can be deduced. Let λ be the radar wavelength and the instantaneous phase of the echoed signal from P_n can be written as

$$\varphi(t) = -\frac{4\pi}{\lambda}R(t). \quad (5)$$

By taking double derivation to (5), the instantaneous Doppler rate $\gamma(t)$ of the echoed signal can be derived as

$$\gamma(t) = -\frac{2v^2(t)}{\lambda R_n} - \frac{2a(t)}{\lambda R_n}(x(t) - x_n) - \frac{2a_r(t)}{\lambda} \quad (6)$$

where $v(t)$ is the instantaneous forward velocity, $a_r(t)$ is the instantaneous cross-track acceleration and $a(t)$ is the instantaneous forward acceleration. Owing to the mechanical inertia of the airborne platform, the variation of the forward velocity is usually small and the impact of $a(t)$ on the Doppler rate can be neglected (Xing et al., 2009). $\gamma(t)$ can be approximated as

$$\gamma(t) \approx -\frac{2v^2(t)}{\lambda R_n} - \frac{2a_r(t)}{\lambda}. \quad (7)$$

Equation (7) reveals the relationship between Doppler rate and motion errors of the QMUAV platform. By using the estimated Doppler rate, the motion error can be calculated and the motion compensation can be implemented accordingly.

4 PROCESSING ALGORITHM

In the QMUAV experiments, it is impossible to mount an expensive INS/GPS equipment on board due to the

small size and limited payload of the platform. Thus, autofocusing technique is used to estimate the motion error from the SAR echoes and the main steps of the processing processing are shown in Fig. 2.

4.1 Doppler Rate Estimation and Compensation

As mentioned in section 3, the motion error is closely related to the Doppler rate that can be estimated from the SAR echoes. However, because the motion error of the QMUAV platform is much more severe than a general aircraft, additional technique needs to be utilized to improve the accuracy of the estimated Doppler rate. As shown in (7), the Doppler rate is varying along the range direction. Thus the range variation of $\gamma(t)$ will be considered by reformulating (7) into

$$\gamma(t)R_n = -\frac{2v^2(t)}{\lambda} - \frac{2a_r(t)}{\lambda}R_n. \quad (8)$$

From (8), it can be seen that $\gamma(t)R_n$ can be regarded as a linearly variant component. Thus, in our QMUAV SAR processing, the SAR data are divided into several range blocks. Generally, it is assumed that when the range size of each block is small, the Doppler rate is regarded as constant along range direction. Meanwhile, the linear variation of $\gamma(t)R_n$ can be observed from different range blocks. Then, linear fitting technique is applied to the estimated Doppler rate from different range blocks to improve the estimating accuracy. Iteration of the above discribed process is performed to refine the accuracy of the estimated Doppler rate.

With the estimated Doppler rate, the cross track motion $a_r(t)$ and the forward velocity $v(t)$ can be separated by using the kinetic characteristic of the QMUAV platform. Generally, the frequency of the forward velocity is very low while the frequency of the cross track acceleration $a_r(t)$ is much higher (Moreira, 1990). Thus, the first and the second terms of (7) can be separated based on their spectral distribution in the frequency domain. Then, both $a_r(t)$ and $v(t)$ can be accordingly calculated.

The map-drift (MD) technique (Carrara et al., 1995; Cumming and Wong, 2005) is employed for the Doppler rate estimation. As reported in (Carrara et al., 1995), the MD can directly estimate the quadratic coefficient of the phase error. Then the obtained estimates are used to apply a one-dimensional correction function to the phase history. Generation and application of the correction function can be readily established once the quadratic error coefficient, corresponding to the Doppler rate of the echoes, is

Table 1: QMUAV SAR Parameters.

Wave Band	Ku Band
Bandwidth	300 MHz
Pulse Repetition Frequency (PRF)	1000 Hz
Synthetic Time Duration	about 20 seconds
Range Centre	150 m
Forward Velocity	4-8 m/s
Flying Altitude	below 100 m

known. Because the MD generally uses the fact that a quadratic phase error (QPE) across the full processing aperture has a differential functional form across two half-length sub-apertures, the full aperture SAR data need to be divided into small data blocks along azimuth direction for MD application.

Because the motion error of the QMUAV is large, the size of the data block along azimuth is usually set to be very small, i.e., about $0.25s$. In this case, it can be assumed that the Doppler rates of the two adjacent sub-apertures are identical, denoted as γ_n . Then, the signals from these two adjacent data blocks are formulated as

$$\begin{cases} s_1(t) = a\left(t - \frac{T}{2}\right) \exp\left(j\pi\gamma_n\left(t - \frac{T}{2}\right)^2\right) \\ s_2(t) = a\left(t + \frac{T}{2}\right) \exp\left(j\pi\gamma_n\left(t + \frac{T}{2}\right)^2\right) \end{cases} \quad (9)$$

By applying FFT to (9), we have

$$\begin{cases} S_1(f) = \int_{-T/2}^{T/2} s_1(t) \exp(-j2\pi ft) dt = \hat{S}_1\left(f + \frac{\gamma_n T}{2}\right) \\ S_2(f) = \int_{-T/2}^{T/2} s_2(t) \exp(-j2\pi ft) dt = \hat{S}_2\left(f - \frac{\gamma_n T}{2}\right) \end{cases} \quad (10)$$

For small data blocks, it can be assumed that (Carra et al., 1995)

$$|S_1(f)|^2 = |S_2(f)|^2. \quad (11)$$

By cross-correlating the two sub aperture signals, the location of the cross correlation peak can be used to measure the relative shift to obtain the quadratic coefficient.

With the estimated Doppler rate, the motion error can be extracted and combined to form the full-aperture function for the motion error compensation. Both phase error and motion induced range cell migration (RCM) are considered in the imaging process. Iterations are also utilized to improve the estimating accuracy.

4.2 PGA Processing

After the quadratic phase error being compensated by Doppler rate estimation, the residual high order phase error needs to be considered to improve the focusing quality of the final image. In the processing, we employ phase gradient autofocus (PGA) which is very useful for high order phase error estimation (Wahl et al., 1994; De Macedo et al., 2008). The success of the technique relies upon four fundamental signal processing steps (Wahl et al., 1994): centre shifting, windowing, phase gradient estimation, and iterative correction. It has been proved that excellent results can be obtained over a wide variety of scene content, and phase error function is achievable if and only if all of the four steps are included in the processing. By following the idea of weighted phase estimation, a weighted ML kernel is employed in the phase gradient estimation (Ye et al., 1999). Weighting technique is based on the contribution adjustments of different samples according to their SCR, which encourages the contribution of high SCR samples in phase gradient estimate. If so, the selection of samples can be much more relaxed and fast convergence can be obtained. The weighted maximum likelihood (WML) kernel is given by

$$\hat{\phi}_e^{WML}(h) = \arg \sum_{k=1}^K \frac{w_k [\text{conj}[s(k, h)] s(k, h+1)]}{\sum_{j=1}^K w_j} \quad (12)$$

where $\hat{\phi}_e^{WML}$ is the estimated phase-error gradient, K is the number of selected range bins, $J+1$ denotes the azimuth length of samples, conj denotes the conjugate operator, and w_k is the weight of the k th range bin. In the PGA estimation, we also use blocking, linear fitting and iterative processing to improve the estimation accuracy (Zhang et al., 2012). After the residual high order phase error being removed, back projection processing is implemented to obtain a well focused SAR image.

5 EXPERIMENTAL RESULTS AND ANALYSIS

In this section, the QMUAV-SAR experimental results are presented and analyzed. Because the size of QMUAV is very small (length: $1.2m$, height: $0.5m$), it is very convenient for launching and landing in a space-constrained environment. A low accurate GPS system is mounted on the top of the QMUAV for navigation. Its measurement accuracy is about $0.1m$,

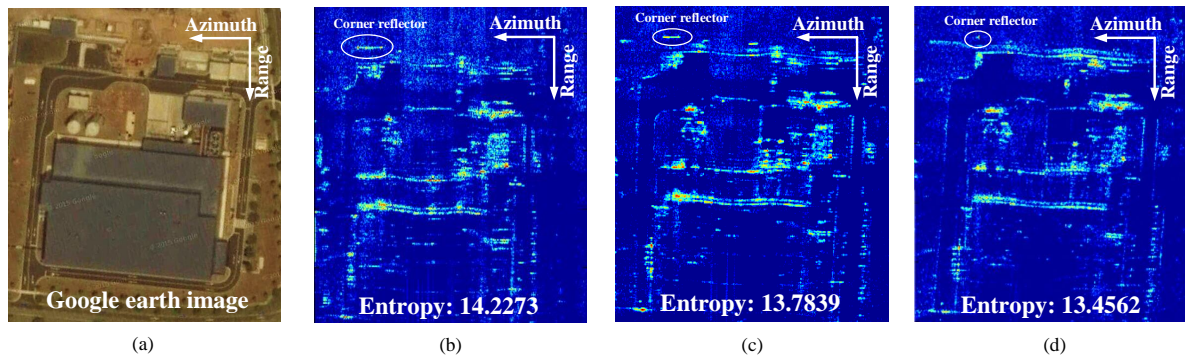


Figure 3: Google earth image and SAR images. (a) Google earth image. (b) QMUAV-SAR image without motion error compensation. (c) QMUAV-SAR image from conventional motion error compensation. (d) QMUAV-SAR image from the proposed method.

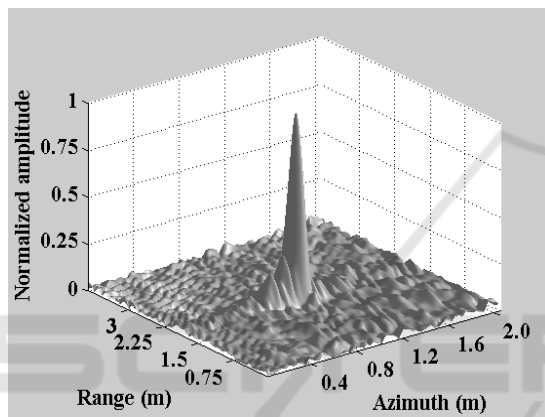


Figure 4: 3D responses of the corner reflector.

which can not meet the requirement of motion error compensation. Therefore, all the motion errors of the QMUAV are to be estimated from the SAR echoes. The above described motion error compensation algorithm is used in the process of SAR imaging formation. Hamming windows are used in the range and the azimuth processing for side lobe suppressions.

Fig. 3 presents the Google earth image and the QMUAV-SAR images. The focusing result without motion error compensation is shown in Fig. 3 (b) showing that the image has serious defocusing and geometrical distortion with an entropy value of 14.2273. With conventional motion error compensation (Moraes, 1990; Xing et al., 2009), the SAR image in Fig. 3 (c) still has some defocusing and geometric distortion with an entropy value of 13.7839. Fig. 3 (d) presents the SAR image obtained from the proposed method that has much reduced defocusing and geometric distortion with a reduced entropy value of 13.4562. From Fig. 3 (d), it can be easily seen that the roads, the round shape objects and the edges of the buildings in the scenario can be easily distinguished in QMUAV SAR image.

To evaluate the focusing quality of the SAR image, the responses of the corner reflector are particularly analyzed. Fig. 4 is the responses of the corner reflector in the SAR image domain. From Fig. 4, it can be seen that the corner reflector is highly focused with well separated main lobe and side lobes. Fig. 5 presents the azimuth and range response of the corner reflector. It is seen that all the side lobes of the response are under 20dB. The shape of the responses of the corner reflector demonstrates the high focusing quality of our QMUAV SAR experiment.

To further examine the spatial resolutions of our QMUAV SAR system, the zoomed azimuth and range responses of the corner reflector are particularly analyzed, as shown in Fig. 6. From the zoomed responses, the azimuth and range resolutions can be evaluated and they are very close to the theoretic values (The theoretic azimuth resolution is $0.15m$ and the theoretic range resolution is $0.44m$), which demonstrates the ability of achieving high spacial resolution of our QMUAV SAR system.

6 CONCLUSION AND FUTURE WORK

This paper presents a motion error compensation algorithm for SAR imaging system on the platform of quad-rotor miniature unmanned aerial vehicle. Because of the severe motion error and the absence of high accurate INS/GPS system on board, we estimate the motion errors from the SAR echoes for compensation. The focusing results are evaluated by the data collected by our real hardware implemented system to show that the proposed error compensation algorithm is effective to achieve high quality SAR images. It should be pointed that the presented image is obtained by the off-line processing mode, i.e., the col-

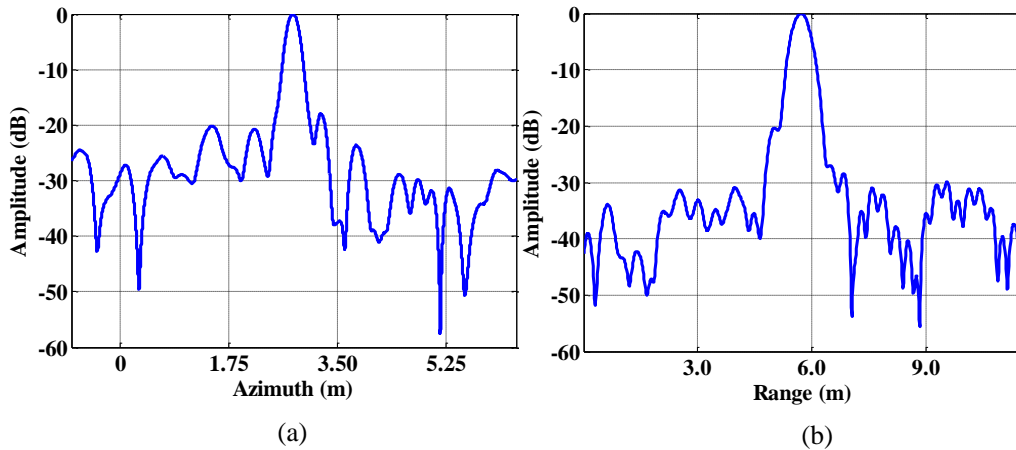


Figure 5: Azimuth response and range response. (a) Azimuth response. (b) Range response.

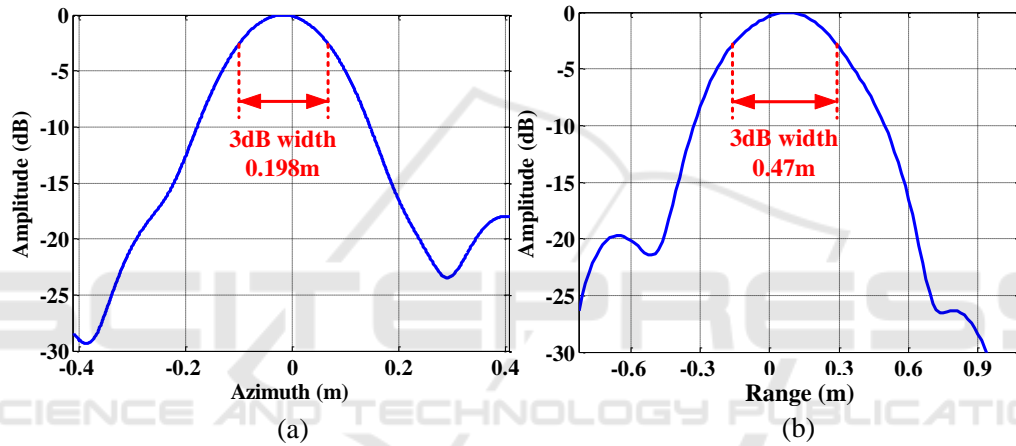


Figure 6: Zoomed responses. (a) Zoomed azimuth response. (b) Zoomed range response.

lected echo data are recorded in an on-board storage and processed on a workstation computer. Development of real-time algorithm and processing system on the QMUAV platform will be our future work.

ACKNOWLEDGEMENTS

The work reported herein was supported by TL@NTU, Singapore. The authors would like to thank the TL@NTU for the flight trials and data support.

REFERENCES

Bao, M., Xing, M., and Li, Y. (2012). Chirp scaling algorithm for geo sar based on fourth-order range equation. *Electronics letters*, 48(1):41–42.
 Carrara, W. G., Goodman, R. S., and Majewski, R. M.

(1995). Spotlight synthetic aperture radar- signal processing algorithms(book). *Norwood, MA: Artech House, 1995.*

Coker, J. and Tewfik, A. (2011). Performance synthesis of uav trajectories in multistatic sar. *Aerospace and Electronic Systems, IEEE Transactions on*, 47(2):848–863.
 Cumming, I. G. and Wong, F. H.-c. (2005). *Digital processing of synthetic aperture radar data: algorithms and implementation*. Artech house.
 De Macedo, K. A. C., Scheiber, R., and Moreira, A. (2008). An autofocus approach for residual motion errors with application to airborne repeat-pass sar interferometry. *Geoscience and Remote Sensing, IEEE Transactions on*, 46(10):3151–3162.
 Desai, M. D. and Jenkins, W. K. (1992). Convolution back-projection image reconstruction for spotlight mode synthetic aperture radar. *Image Processing, IEEE Transactions on*, 1(4):505–517.
 Dydek, Z., Annaswamy, A., and Lavretsky, E. (2013). Adaptive control of quadrotor uavs: A design trade study with flight evaluations. *Control Systems Technology, IEEE Transactions on*, 21(4):1400–1406.

- Huang, L., Qiu, X., Hu, D., and Ding, C. (2011). Focusing of medium-earth-orbit sar with advanced nonlinear chirp scaling algorithm. *Geoscience and Remote Sensing, IEEE Transactions on*, 49(1):500–508.
- Lara, D., Romero, G., Sanchez, A., Lozano, R., and Guerrero, A. (2010). Robustness margin for attitude control of a four rotor mini-rotorcraft: Case of study. *Mechatronics*, 20(1):143–152.
- Liao, Y., Xing, M.-d., Zhang, L., and Bao, Z. (2013). A novel modified omega-k algorithm for circular trajectory scanning sar imaging using series reversion. *EURASIP Journal on Advances in Signal Processing*, 2013(1):1–12.
- Moreira, J. (1990). A new method of aircraft motion error extraction from radar raw data for real time motion compensation. *Geoscience and Remote Sensing, IEEE Transactions on*, 28(4):620–626.
- Munson, D. C., O'Brien, J. D., and Jenkins, W. K. (1983). A tomographic formulation of spotlight-mode synthetic aperture radar. *Proceedings of the IEEE*, 71(8):917–925.
- Sun, G., Xing, M., Xia, X.-G., Wu, Y., and Bao, Z. (2013). Robust ground moving-target imaging using deramp-keystone processing. *Geoscience and Remote Sensing, IEEE Transactions on*, 51(2):966–982.
- Wahl, D., Eichel, P., Ghiglia, D., and Jakowatz, C.V., J. (1994). Phase gradient autofocus—a robust tool for high resolution sar phase correction. *Aerospace and Electronic Systems, IEEE Transactions on*, 30(3):827–835.
- Xing, M., Jiang, X., Wu, R., Zhou, F., and Bao, Z. (2009). Motion compensation for uav sar based on raw radar data. *Geoscience and Remote Sensing, IEEE Transactions on*, 47(8):2870–2883.
- Xu, G., Xing, M., Zhang, L., and Bao, Z. (2013). Robust autofocusing approach for highly squinted sar imagery using the extended wavenumber algorithm. *Geoscience and Remote Sensing, IEEE Transactions on*, 51(10):5031–5046.
- Yang, L., Bi, G., Xing, M., and Zhang, L. (2015). Airborne sar moving target signatures and imagery based on lvd. *Geoscience and Remote Sensing, IEEE Transactions on*, 53(11):5958–5971.
- Yang, L., Xing, M., Wang, Y., Zhang, L., and Bao, Z. (2013). Compensation for the nsrsm and phase error after polar format resampling for airborne spotlight sar raw data of high resolution. *Geoscience and Remote Sensing Letters, IEEE*, 10(1):165–169.
- Ye, W., Yeo, T. S., and Bao, Z. (1999). Weighted least-squares estimation of phase errors for sar/isar autofocus. *Geoscience and Remote Sensing, IEEE Transactions on*, 37(5):2487–2494.
- Zeng, T., Li, Y., Ding, Z., Long, T., Yao, D., and Sun, Y. (2015). Subaperture approach based on azimuth-dependent range cell migration correction and azimuth focusing parameter equalization for maneuvering high-squint-mode sar. *Geoscience and Remote Sensing, IEEE Transactions on*, 53(12):6718–6734.
- Zhang, L., Qiao, Z., Xing, M.-d., Yang, L., and Bao, Z. (2012). A robust motion compensation approach for uav sar imagery. *Geoscience and Remote Sensing, IEEE Transactions on*, 50(8):3202–3218.
- Zhao, B., Xian, B., Zhang, Y., and Zhang, X. (2015). Nonlinear robust adaptive tracking control of a quadrotor uav via immersion and invariance methodology. *Industrial Electronics, IEEE Transactions on*, 62(5):2891–2902.
- Zhao, L., Wang, L., Bi, G., and Yang, L. (2014). An autofocus technique for high-resolution inverse synthetic aperture radar imagery. *Geoscience and Remote Sensing, IEEE Transactions on*, 52(10):6392–6403.
- Zhou, S., Bao, M., Zhou, P., Xing, M.-D., and Bao, Z. (2011). An imaging algorithm for missile-borne sar with downward movement based on azimuth nonlinear chirp scaling. *Dianzi Yu Xinxi Xuebao (Journal of Electronics and Information Technology)*, 33(6):1420–1426.
- Zhou, S., Xing, M., Xia, X.-G., Li, Y., Zhang, L., and Bao, Z. (2013). An azimuth-dependent phase gradient autofocus (apga) algorithm for airborne/stationary bisar imagery. *Geoscience and Remote Sensing Letters, IEEE*, 10(6):1290–1294.